JOURNAL OF MATERIALS SCIENCE 26 (1991) 5149–5154

Influence of preform surface treatments on the strength of fluorozirconate fibres

P. C. PUREZA, P. H. KLEIN, W. I. ROBERTS*, I. D. AGGARWAL
US Naval Research Laboratory, Washington, DC 20375, USA

Zirconium fluoride (ZrF_4)-based glass preforms made by the rotational casting process were treated prior to fibre drawing to eliminate pre-existing defects. Emphasis was given to the removal of external defects by different surface preparation methods which include mechanical polishing, and chemical etching in 0.2 M H_3BO_3 solution as well as microwave-assisted plasma fluorination. The strength of the fibres was measured using both bending and dynamic loading tests. Fluorine exposure increased the median tensile strength by an additional 20%. As expected, the Weibull distribution for bending tests was shifted to the higher strength range, and was generally a factor of two more than in the dynamic tensile measurements.

1. Introduction

Heavy-metal fluoride (HMF) glass fibres have high transparency ranging from the near-UV ($\sim$ 0.3 μm) to the mid-IR ($\sim$ 7.0) region depending on compositions [1]. Due to their excellent optical properties, fluoride fibres are potential candidates for a wide range of military as well as industrial applications including ultra-low loss, long length repeaterless optical communication links. The intrinsic minimum loss for fluoride glasses is predicted to be of the order of 10^{-2} to 10^{-3} dB km^{-1} at the $\sim$ 2–4 μm band [2]. Although the optical loss for fluoride fibres is still higher than for silicates, progress in attenuation reduction has already been reported [3] as a result of improvements in materials processing and fibre/preform preparations. However, if these fibres are to be deployed in any field applications, its mechanical survivability must also be addressed.

The mechanical properties of HMF glass are currently being investigated by several researchers. Mecholsky *et al.* [4], for instance, had measured fracture toughness for these materials and reported a value of $K_{IC} \sim 0.5$ MPa $m^{1/2}$, which is comparable to that of high-silica fibres ($K_{IC} \sim 0.72$ MPa $m^{1/2}$). Also recently, Freitas *et al.* [5] studied Raman spectra behaviour of ZBLAN (Zr–Ba–La–Al–Na fluoride) fibres under tensile stress of up to 300 MPa at room temperature. For fluorozirconates, moduli of elasticity are typically in the 55–60 GPa [6] range. Obviously, the practical strength of fluoride fibres can compare favourably with that of silicates.

In general, two types of fracture-causing defects have been identified in optical fibres. Intrinsic or matrix defects consist primarily of inhomogeneities, bubbles, microcrystals, phase separation and other inclusions. Extrinsic or surface defects are typically pits, scratches, microcracks, microcrystals and other foreign particles. Likewise, the presence of atmospheric water can introduce defects especially during fibre drawing or reheating. In earlier work, Klein [7] and also Nakai *et al.* [8] demonstrated the effects of NF_3-containing argon plasma on the optical characteristics of ZBLAN preform slices by comparing the OH absorption bands at $\sim$ 2.9 μm.

One of the many constraints in the successful drawing of continuous-length fluorozirconate fibres is its steep temperature–viscosity relationship, giving rise to a very narrow working temperature range (i.e. $\Delta t = t_x - t_g$) compared to silicate glasses. For halide glasses, Δt is $\leq$ 100 °C and should be kept as small as 5 °C in practice. Hence, accurate control of the draw temperature and atmosphere is critical if long-length, low-loss and high-strength fibres are to be fabricated. Due to its relatively poor chemical durability, fluoride fibres are usually drawn in a clean, ultra-dry inert environment although reactive-atmosphere drawing is also under consideration. For this reason, Teflon FEP has been widely used as a protective coating for HMF fibres [9]. Nakata *et al.* [10], however, had shown quite convincingly that water can indeed permeate through and remain trapped in the FEP matrix, eventually attacking the glass surface. Furthermore, they theorized a hydration mechanism taking place irreversibly at the fibre surface and causing damage.

Fluoride preforms are usually prepared by the casting technique; hence surface defects from contact with the mould cannot be avoided. In contrast, silica preforms are made via the modified chemical vapour deposition (MCVD) process which imparts a nearly defect-free and highly polished surface. Removal of bulk defects in the casted preforms is difficult once it is made. It is therefore the object of this paper to improve and compare the tensile strengths of fibres drawn from preforms subjected to different surface treatments.

* *Present address*: SFA Inc., 1401 McCormick Drive, Landover, MD 20785, USA.

0022–2461/91 $03.00 + .12

2. Experimental procedure

Multimode fibre preforms with a core-cladding structure (NA ~ 0.14) were prepared from ZBLAN-type glasses via the rotational casting techniques described by Tran *et al.* [11]. Three different preform surface conditioning methods were used, namely (a) mechanical polishing, (b) chemical etching in 0.2 M H_3BO_3 in 1.0 N HCl and (c) a combination of (a) and (b) followed by fluorination in a microwave-assisted NF_3-containing Ar plasma [12]. In method (a), selected preforms underwent a series of polishing steps using SiC paper and ending with 0.25 μm diamond paste as reported in a previous publication [13]. The second method involved etching in 0.2 M H_3BO_3 in 1.0 N HCl for ~ 10 min followed by a rinsing steps using 1.0 N HCl, distilled water, acetone and hexane in turn. Exposure of preforms to active fluorine was done using a specially-fitted, commercially available 750 W microwave oven as described elsewhere [12]. Teflon lines were used for the Ar and NF_3 gases. The preform was supported inside a demountable PFA chamber during the treatments, then sealed under pressure and immediately transferred to the drawing tower.

Gas flow rates were controlled by mass flow controllers at the rates of 45 ml min^{-1} of Ar and 18 ml min^{-1} of NF_3. The system was initially purged with Ar and evacuated down to < 0.2 Pa where it was held for ~ 45 min to exclude ambient air. The total pressure was reduced to 5–8 Pa upon introduction of the gases. The chamber was placed outside the microwave oven to keep the preform as close as possible to room temperature. Treatment time was approximately 30 min.

Fibres were drawn at 10 m min^{-1} at 312 °C under a constant tension of 0.20 N and coated with DeSoto UV-curable epoxy-acrylates. The fibre diameter was nominally at 130 μm with a 60 μm thick protective coating. Preforms were treated, drawn and tested under similar conditions within 24 h. Dynamic tensile strength tests on 1.0 m gauge-length fibres was carried out at a constant strain rate of 1.0 mm min^{-1} using the instrument described previously [5]. A simple bending technique [14] for measuring fibre strength was also employed in parallel, using samples 20 cm long. 40 replicate measurements were made for each fibre sample using both testing methods under room conditions of 25 °C and 60% RH. Additionally, to correlate the strength behaviour with surface chemistry effects, 2.11 mm thick polished preform slices were prepared. Infrared (IR) spectra were then taken using a double-beam spectrophotometer (PE Model 580B) after exposing the samples at 25 °C for 40 h to 81% RH in the air over saturated aqueous ammonium sulphate. Absorption spectra were recorded after each of the three 30 min exposures to plasma-generated active fluorine.

3. Results and discussion

3.1. Surface defects

Some of the most common types of extrinsic defect in casted fluoride preforms are shown in Figs 1 to 3. Fig. 1 shows pits of different sizes ranging from 8 to 26 μm after chemical etching. The exact source of these defects is not easy to identify but it can be narrowed down to a poor-quality mould surface or sites vacated by crystallites. Bubbles at or near the surface are another defect which can negate the accuracy of fibre drawing systems and hence adversely affect the integrity of the fibre. Fig. 2 is an enlarged view of an isolated tear-drop-shaped, near-surface bubble after polishing a ~ 50 μm layer off the preform. In this case, the thinner end of the bubble near the surface was opened up by polishing. The round-bottom end, which was almost spherical, measures about 350 μm across. Crystals of yet unknown composition were also observed inside this bubble. Fig. 3 shows a cluster of bubbles before and after redrawing at 312 °C. This was done intentionally to see how surface bubbles behave during the fibre drawing process. Bubbles, as shown in Fig. 3a, were deformed from (a) spherical (~ 560 μm diameter) to elliptical as in (b) 670 μm × 460 μm and (c) 970 μm × 480 μm in size, as the glass underwent viscous shearing at the neckdown region. Finally, in Fig. 3b, the bubbles were elongated to 2200 μm × 290 μm but did not completely collapse as the fibre left the hot zone.

Other forms of defect observed in fluoride preforms include contaminants such as metallic particles and

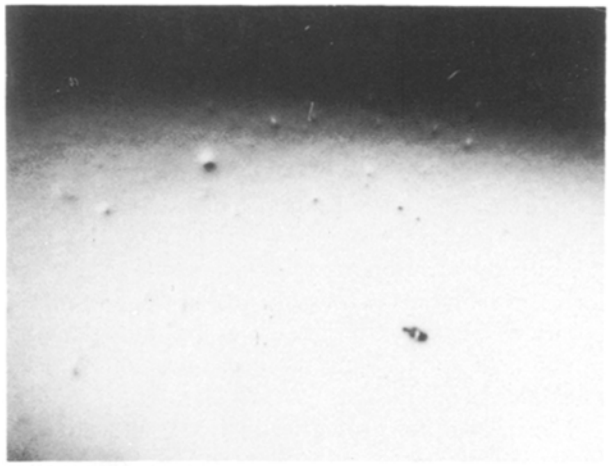

Figure 1 Preform surface showing pits of different sizes ranging from 8 to 26 μm after etching in 0.2 M H_3BO_3/1.0 N HCl (50 ×).

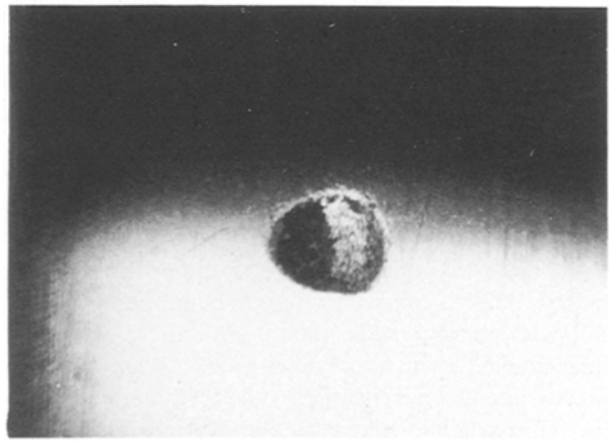

Figure 2 An isolated near-surface bubble, ~ 350 μm in size and after mechanical polishing (50 ×).

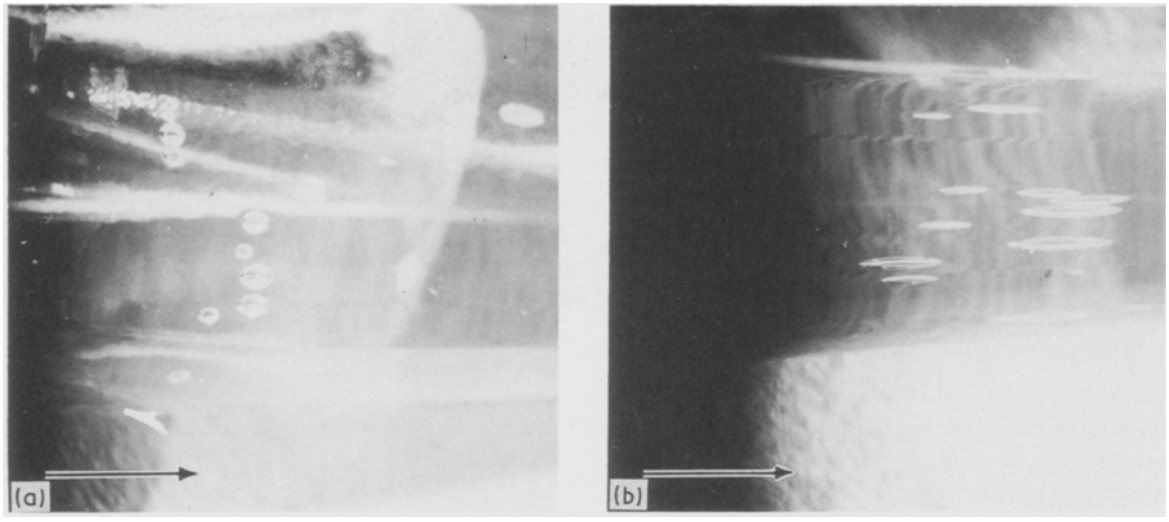

Figure 3 Effects of reheating/drawing at 312 °C on surface bubbles: (a) before and during reheating, shape of bubbles changed from spherical to elliptical; (b) bubbles were stretched near the neckdown–fibre transition point. Arrows indicate direction of drawing.

scratches from the mould. Scratches shown in Fig. 2 were from the last two polishing steps. Platinum and graphite particles have also been identified. Continued improvements in all aspects of processing are expected to help eliminate these defects, thereby increasing fibre strength as well as lowering optical attenuation.

3.2. Strength measurements

The Weibull distribution function is well known and is widely used to characterize fracture stress variability in optical glass fibres. This approach is based on the "weakest-link" concept [15], which assumes that fracture will occur at the weakest volume element of the specimen at a given load. Thus, a fibre will fail when the critical fracture stress at a dominant flaw is reached. Measurement is however not trivial due to the random nature of the flaw size and spatial distribution. In its general form, the Weibull probability function is given by the equation

$$F = 1 - \exp\left[- \left(\frac{\sigma_f - \sigma_u}{\sigma_0} \right)^m \right]$$

where σ_f, σ_u, m and σ_0 are the fracture stress, minimum strength, Weibull shape and strength scaling parameters, respectively.

The results from dynamic and bending strength measurements are summarized in a Weibull failure probability plot in Fig. 4 using regression analysis. Points were omitted for clarity. In dynamic loading tests, the fracture load for a given sample is simply divided by the fibre cross-sectional area at the break point. On the other hand, the maximum stress in bending derived by Matthewson *et al.* [16] is expressed as follows

$$\sigma_{max} = 1.198 E \left(\frac{2r}{D - d} \right)$$

where r, D and d are the fibre radius, face-plate distance at the instant of fracture and the overall coated fibre diameter respectively. The constant ($k = 1.198$) is a geometric shape factor determined by

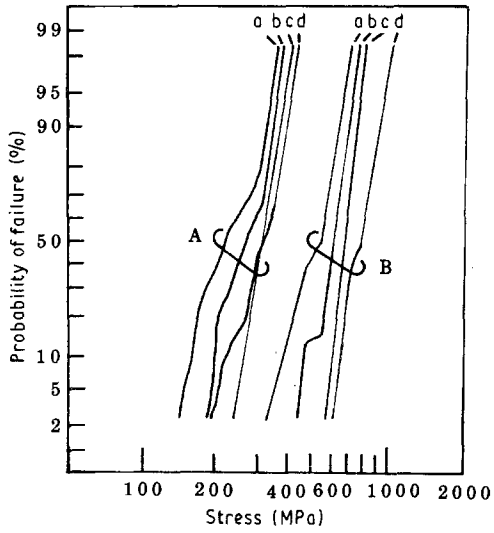

Figure 4 Weibull failure probability as a function of stress measured in air at 25 °C, 60% relative humidity. Preform surface treatments: (a) mechanical polishing, (b) chemical etch, (c, d) mechanical polishing/etch plus plasma-activated fluorine. (A) Dynamic tensile loading; (B) bending strength measured under the same conditions. (Curves b, c and d from [12].)

the previous authors. For the present work, the constant in the above equation is assumed to be unity. Hence, the results shown in curves B of Fig. 4 were underestimated by $\sim 20\%$. Matthewson *et al.* [16] gave a detailed analysis of the many drawbacks of the bending method and its implications in strength prediction. Discretion must therefore be observed in the interpretation of the bending strength data. In particular, the gauge length under high stress in bending is small (typically $\leq$ 1.0 mm) compared to that in tensile loading, and can almost account for the 2:1 difference in observed strength values. In addition, stress is at its maximum only at the outer radius of the fibre while the inner radius is under compression.

As shown in Fig. 4, the strength in both tension and bending increased with each successive surface treatment in the order indicated; that is, mechanical polishing, chemical etching and plasma fluorination. Fibres a, b and d in curves A of Fig. 4 show a

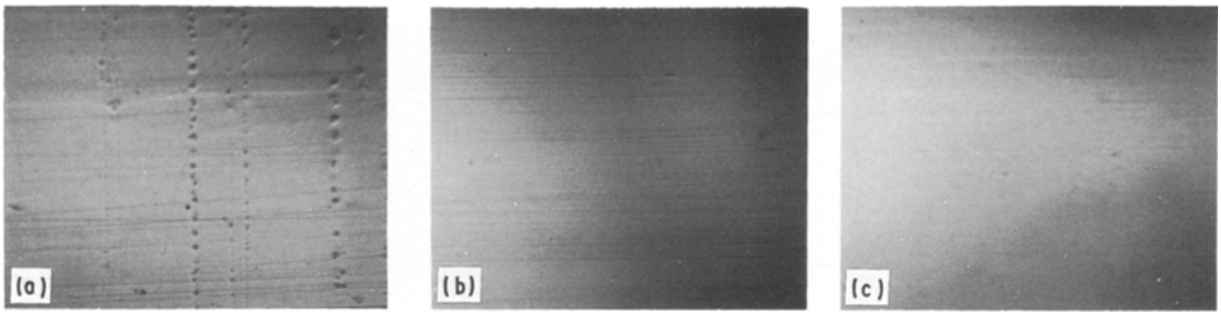

Figure 5 Effects of preform surface treatments: (a) untreated or "fresh" preform, (b) mechanically polished, (c) polished and etched.

multimodal behaviour suggesting the existence of at least two failure mechanisms associated with flaw size distribution. Note that a similar profile is displayed by the bending results in curves B. The low failure mode in dynamic loading has a distinct cut-off at $\sim 65\%$ failure probability, representing the larger flaw-size population. Furthermore, the strength variability as indicated by the S-shaped curve signifies that, for this region alone, different failure or flaw types are responsible. It is also apparent that the dominant low-strength failure modes characterized by the S-curves were all displaced towards the higher strength region. In comparison, the high failure mode was increased only slightly as shown by the slopes of the lines. Presumably, the flaw distribution is shifted to higher strength in accordance with the methods of surface treatments used. For instance, mechanical polishing alone removed fewer of the defects responsible for low-stress failure than did chemical etching. Polishing and etching in boric acid can be combined with active fluorination to further enhance the fibre strength as indicated by fibres c and d. At 50% probability, this corresponds to an increase in strength of ~ 20–30%. Active fluorine treatment alone results in slightly weaker fibres than polishing, as shown in previous work [12].

As mentioned earlier, the surface of a fresh preform can contain several types of defect which must be eliminated prior to fibre drawing. The immediate effects of the treatments used are shown in Fig. 5. Contraction marks, mostly perpendicular to the preform axis, induced by the spin-casting process are also prominent in the photo. The scratches were measured to be in the range of a few micrometres up to $\sim 30\ \mu m$ in width. Mechanical polishing resulted in a surface with scratches in the 0.25–2.0 μm range (Fig. 5b), typically obtained from the last two polishing steps. In Fig. 5c, most of the scratches were removed after etching in 0.2 M H_3BO_3 although some residual pits remained.

The Weibull plot in curves A of Fig. 4 gives the minimum strength for 1.0 m gauge-length samples in the 150–255 MPa range and an observed upper strength limit of 380–440 MPa. The flaw size in these fibres, which is also related to the fracture toughness of the materials, can then be estimated from the Equation [17]

$$K_{IC} = \sigma(\pi a)^{1/2}$$

where K_{IC}, σ and a are the critical stress intensity factors, fracture stress and crack depth, respectively. Using the K_{IC} value for HMF fibres reported by Mecholsky *et al.* [4] gives an estimated crack depth of 1.3–3.6 μm for the low-strength distribution and 0.4–0.6 μm for the maximum strength range. Scanning electron microscopy (SEM) was hence carried out in an attempt to determine the cause or origin of fracture. Fig. 6 is an SEM micrograph of a fractured fibre taken at the low end of the Weibull plot (curves A of Fig. 4). It is evident from the familiar mirror–mist–hackle pattern that fracture originated from the surface and propagated radially. The flaw was identified as a "micro-pit" arising most likely from a site vacated by a crystallite of yet unknown composition or structure. The mirror radius (r_m) for this fracture was about 15 μm. Krohn and Hasselman [18] estimated the flaw size with circular shape to be $\sim 0.1\ r_m$ in soda–lime–silica glass. Assuming that the same relationship is also valid for fluorozirconates, then for the fibre shown in Fig. 6 the flaw size responsible for the low-strength failure is $\sim 1.5\ \mu m$. This is in good agreement with the 1.3–3.6 μm range calculated previously.

Interpretation of the Weibull distribution for the bending test results in curves B of Fig. 4 is somewhat

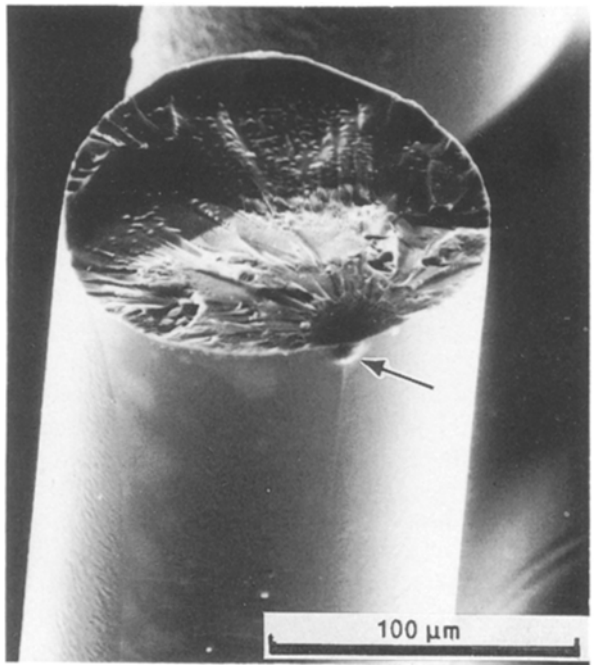

Figure 6 Scanning electron micrograph of a low-failure fibre end showing origin of fracture. Mirror–mist–hackle pattern was initiated from the surface.

less complicated. As in tensile loading, the effect of the surface treatments is to shift the strength towards a higher region. Chemical etching is slightly more effective than mechanical polishing in the removal of surface defects, but when combined with active fluorine exposure the median strength in bending was increased by 20–50%. The maximum strength observed in bending was 1.2 GPa for fibre d or roughly three times that of the dynamic test results for the same fibre.

Stress corrosion or chemical durability is another mechanism that is well documented in silica fibres and has recently been extended by other researchers [19–21] to include the fluorozirconate glasses. The work of Simmons and Simmons [19] on the corrosion behaviour of ZrF_4 glasses in aqueous environments showed that these materials are readily attacked by water even at ambient temperatures, forming a thick hydrated layer covered with crystal deposits, later identified by X-ray diffraction as ZrF_4 and possibly as $ZrBaF_6$. On the other hand, HMF glasses are quite stable in the presence of atmospheric water [20] but highly reactive at elevated temperatures near or above the glass transition [22] and most notably at the reheating or fibre drawing temperatures. It is therefore crucial to draw these fibres in an ultra-dry environment to minimize–OH absorption loss [23] and to maximize its mechanical strength. Infrared spectra of preform slices (Fig. 7) show that surface hydroxides were removed by fluorine exposure, suggesting that strength degradation may also involve hydroxide ions.

3.3. Absorption spectra

The transmission wavelength of interest at 2.55 μm is close to the hydroxide stretching absorption around 2.9 μm (3440 cm^{-1}). A composite of these spectra, covering the 2.5–4.0 μm (4000–2500 cm^{-1}) range, is shown in Fig. 7. The baseline is the mean of absorbances where the glass is relatively transparent at 4000 and 2500 cm^{-1}.

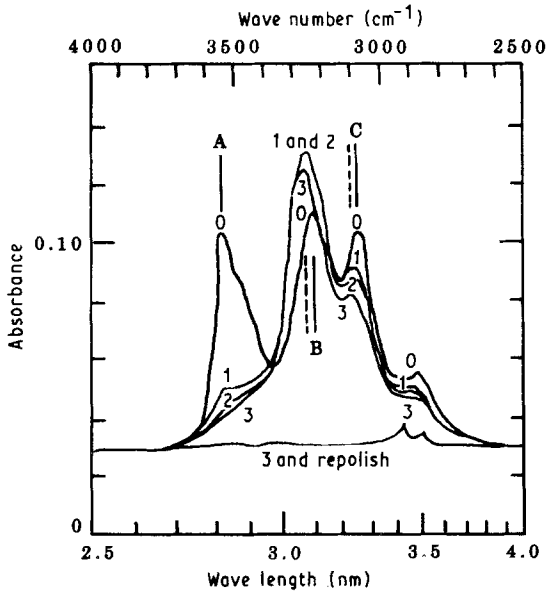

Figure 7 Absorption spectra of a polished preform slice, 2.11 mm thick, which had been exposed to 81% RH for 40 h. Numbers of subsequent 30 min exposures to plasma-activated fluorine are indicated by small numerals [12].

The three narrow peaks A, B and C of Fig. 7 fall within the limits of the broad absorption bands observed after fluoride-glass hydrolysis in steam [21, 24, 25] and liquid water [20, 26]. Continued humid-air hydrolysis could cause these three peaks to grow and coalesce into the broad bands seen in the other studies.

Peak A, a composite of a large absorption at 2.82 μm (3541 cm^{-1}) and a shoulder at 2.88 μm (3476 cm^{-1}) is virtually removed by active-fluorine treatment. The shoulder may be identified with O–H stretching peaks found in the 3440–3448 cm^{-1} range in ZBLAN glasses exposed to liquid water [20, 26] or remelted in Ar after water-vapour hydrolysis [8]. From similar evidence [27, 28] it is possible to ascribe the 3441 cm^{-1} peak to O–H stretching vibrations, modified by hydrogen-bonded HF.

Peaks B and C both shift in wavelength after fluorine exposure. An argument can be made for these shifts to reflect reactions of water of hydration with fluorine or HF. Evidence is stronger in the case of peak B: its wavelength shifts from 3229 to 3555 cm^{-1}; $H_3^+ \cdots F^-$ structures absorb strongly at 3255 cm^{-1} [29]; its intensity initially increases (formation of $H_3O^+ \cdots F^-$), then decreases as water of hydration is removed. Further work will be required before the species responsible for peak C can be elucidated.

4. Conclusion

Near-surface and surface defects induced by preform casting are a dominant source of low-stress failure in fluorozirconate fibres. Examination of the fractured ends by SEM confirmed the origin of failure to be surface-activated as shown by the classic mirror–mist–hackle pattern. Removal of those pre-existing defects prior to fibre drawing is necessary to improve fibre strength. By combining mechanical polishing and etching of preforms in boric acid with fluorine treatment from an NF_3–Ar plasma, an additional ~ 20% improvement in median tensile strength and as much as ~ 50% in bending were observed. The values from bending tests were typically two to three times those from dynamic tensile measurements. This difference can be attributed to the extremely small volume of fibre subjected to high stress. Nevertheless, the Weibull plots for both tensile and bending show a similar trend as a direct consequence of the surface treatments utilized, and hence the bending technique can still be used to at least qualitatively compare surface effects on fibre strength and to characterize the flaw distribution as well.

IR absorption spectra show the effectiveness of active fluorine exposures in the removal of hydroxide-related bands at ~ 2.9 μm. Hydroxide removal may not be the only chemical change on the surface resulting from fluorination. Formation of complexes may be another mechanism contributing to strength enhancement.

References

1. D. C. TRAN, G. H. SIGEL Jr and B. BENDOW, *J. Lightwave Technol.* **LT-2** (5) (October 1984).
2. S. SHIBATA, M. HORIGUCHI, K-JINGUJI, S. MITACHI, T. KANAMORI and T. MANABE, *Electron. Lett.* **17** (1981) 775.
3. M. W. MOORE, P. W. FRANCE, S. F. CARTER and J. R. WILLIAMS, *Mater. Sci. Forum* **32–33** (1988) 457.
4. J. J. MECHOLSKY, J. LAU, J. D. MACKENZIE, D. C. TRAN and B. BENDOW, in Extended Abstracts of 2nd International Symposium on Halide Glasses, Troy, New York, 1983, p. 32.
5. J. A. FRIETAS Jr, P. C. PUREZA, W. I. ROBERTS, U. STROM and I. D. AGGARWAL, *Mater. Sci. Forum* **32–33** (1988).
6. B. BENDOW, in Final Report to Naval Ocean Systems Center, San Diego, CA (1984).
7. P. H. KLEIN, *Mater. Sci. Forum* **19–20** (1987) 193.
8. T. NAKAI, N. NORIMATSU and Y. NODA, *Opt. Laser Technol.* **19** (1987) 271.
9. S. MITACHI, S. SHIBATA and T. MANABE, *Electron. Lett.* **17** (1980) 128.
10. A. M. NAKATA, J. LAU and J. D. MACKENZIE, *J. Non-Cryst. Solids* **74** (1985) 229.
11. D. C. TRAN, C. F. FISHER and G. H. SIGEL Jr, *Electron. Lett.* **17** (1982) 657.
12. P. H. KLEIN, P. C. PUREZA, W. I. ROBERTS and I. D. AGGARWAL, *Mater. Sci. Forum* **32** (1988) 571.
13. P. C. PUREZA, D. T. BROWER and I. D. AGGARWAL, *J. Amer. Ceram. Soc.* **72** (1989) 1980.
14. P. W. FRANCE, M. J. PARADINE, M. H. REEVE and G. R. NEWNS, *J. Mater. Sci.* **15** (1980) 825.
15. W. WEIBULL, *J. Appl. Mech.* **18** (3) (1951) 293.
16. M. J. MATTHEWSON, C. R. KURKJIAN and S. T. GULATI, *J. Amer. Ceram. Soc.* **69** (1986) 815.
17. D. KALISH, P. L. KEY, C. R. KURKJIAN, B. K. TARIYAL and T. T. WANG, in "Optical Fiber Telecommunications", edited by S. E. Miller and A. G. Chynoweth (1979) pp. 401–4.
18. D. A. KROHN and D. P. H. HASSELMAN, *J. Amer. Ceram. Soc.* **54** (1971) 411.
19. C. J. SIMMONS and J. H. SIMMONS, *ibid.* **69** (1986) 661.
20. E. O. GBOGI, K. H. CHUNG, C. T. MOYNIHAN and M. G. DREXHAGE, *ibid.* **64** (1981) C-51.
21. S. R. LOEHR, A. J. BRUCE, R. MOSSADEGH, R. H. DOREMUS and C. T. MOYNIHAN, *Mater. Sci. Forum* **5** (1985) 311.
22. D. TREGOAT, G. FONTENEAU and J. LUCAS, *ibid.* **5** (1985) 323.
23. Y. OHISHI, S. MITACHI and S. TAKAHASHI, *Mater. Res. Bull.* **19** (1984) 673.
24. S. R. LOEHR, K. H. CHUNG and C. T. MOYNIHAN, *J. Amer. Ceram. Soc.* **71** (1988) C-46.
25. S. MITACHI, G. FONTENEAU, P. S. CHRISTENSEN and J. LUCAS, *J. Non-Cryst. Solids* **92** (1987) 326.
26. M. Le TOULLEC, C. J. SIMMONS and J. H. SIMMONS, *J. Amer. Ceram. Soc.* **71** (1988) 219.
27. T. NAKAI, Y. MIMURA, H. TOKIWA and O. SHINBORI, *J. Lightwave Technol.* **LT-4** (1986) 87.
28. G. E. WALRAFEN and P. H. KLEIN, *J. Chem. Phys.* **86** (1987) 6515.
29. P. A. GIGUERE and S. TURRELL, *J. Amer. Chem. Soc.* **102** (1980) 5473.

Received 29 June
and accepted 20 December 1990